

# The Dynamical State of Dark Matter Haloes in Cosmological Simulations I: Correlations with Mass Assembly History

Chris Power<sup>1,2</sup>, Alexander Knebe<sup>3</sup> & Steffen R. Knollmann<sup>3</sup>

<sup>1</sup>International Centre for Radio Astronomy Research, University of Western Australia, 35 Stirling Highway, Crawley, Western Australia 6009, Australia

<sup>2</sup>Department of Physics & Astronomy, University of Leicester, University Road, Leicester LE1 7RH, United Kingdom

<sup>3</sup>Departamento de Física Teórica, Módulo C-15, Facultad de Ciencias, Universidad Autónoma de Madrid, 28049 Cantoblanco, Madrid, Spain

## ABSTRACT

Using a statistical sample of dark matter haloes drawn from a suite of cosmological  $N$ -body simulations of the Cold Dark Matter (CDM) model, we quantify the impact of a simulated halo's mass accretion and merging history on two commonly used measures of its dynamical state, the virial ratio  $\eta$  and the centre of mass offset  $\Delta r$ . Quantifying this relationship is important because the degree to which a halo is dynamically equilibrated will influence the reliability with which we can measure characteristic equilibrium properties of the structure and kinematics of a population of haloes. We begin by verifying that a halo's formation redshift  $z_{\text{form}}$  correlates with its virial mass  $M_{\text{vir}}$  and we show that the fraction of its recently accreted mass and the likelihood of it having experienced a recent major merger increases with increasing  $M_{\text{vir}}$  and decreasing  $z_{\text{form}}$ . We then show that both  $\eta$  and  $\Delta r$  increase with increasing  $M_{\text{vir}}$  and decreasing  $z_{\text{form}}$ , which implies that massive recently formed haloes are more likely to be dynamically unrelaxed than their less massive and older counterparts. Our analysis shows that both  $\eta$  and  $\Delta r$  are good indicators of a halo's dynamical state, showing strong positive correlations with recent mass accretion and merging activity, but we argue that  $\Delta r$  provides a more robust and better defined measure of dynamical state for use in cosmological  $N$ -body simulations at  $z \simeq 0$ . We find that  $\Delta r \lesssim 0.04$  is sufficient to pick out dynamically relaxed haloes at  $z=0$ . Finally, we assess our results in the context of previous studies, and consider their observational implications.

**Key words:** methods:  $N$ -body simulations – galaxies: formation – galaxies: haloes – cosmology: theory – dark matter – large-scale structure of Universe

## 1 INTRODUCTION

One of the fundamental assumptions underpinning modern theories of galaxy formation is that galaxies form and evolve in massive virialised haloes of dark matter (White & Rees 1978; White & Frenk 1991). Characterising the properties of these haloes is an important problem, both theoretically and observationally, and its study has been one of the main objectives of cosmological  $N$ -body simulations over the last two decades. The majority of these simulations have modeled halo formation and evolution in a purely Cold Dark Matter (CDM) universe (cf. Springel et al. 2006), with the focus primarily on their equilibrium structure (cf. Diemand & Moore 2009). Various studies have revealed that CDM haloes in dynamical equilibrium are triaxial structures (e.g. Bailin & Steinmetz 2005) supported by velocity dispersion rather than rotation (e.g. Bett et al. 2007), with mass profiles that are divergent down to the smallest resolvable radius (e.g. Diemand et al. 2008; Stadel et al. 2009; Navarro et al. 2010) and an abundance of substructure (e.g. Diemand et al. 2007; Springel et al. 2008; Gao et al. 2011).

The qualification that a halo is in dynamical equilibrium is a

particularly important one when seeking to characterise the structure and kinematics of simulated haloes in cosmological simulations. Previous studies have shown that dynamically unrelaxed haloes tend to have lower central densities (see, for example, Tormen et al. 1997; Macciò et al. 2007; Romano-Díaz et al. 2007) and higher velocity dispersions (see, for example, Tormen et al. 1997; Hetzner & Burkert 2006; D'Onghia & Navarro 2007) than their dynamically relaxed counterparts. This means that a dynamically unrelaxed halo is likely to have a measurably lower concentration  $c_{\text{vir}}$  and higher spin parameter  $\lambda$  than its dynamically relaxed counterpart (see, for example, Gardner 2001; Macciò et al. 2007), and so care must be taken to avoid contaminating halo samples with dynamically unrelaxed systems when measuring, for example, spin distributions (e.g. Bett et al. 2007; Macciò et al. 2007; D'Onghia & Navarro 2007; Knebe & Power 2008) and the correlation of halo mass and concentration  $c_{\text{vir}} - M_{\text{vir}}$  (e.g. Macciò et al. 2007; Neto et al. 2007; Gao et al. 2008; Prada et al. 2011).

Yet haloes do not exist in isolation, and the degree to which they are dynamically relaxed or unrelaxed bears the imprint of both their environment and their recent mass assembly and merg-

ing history. As previous studies have shown, dynamically unrelaxed haloes tend to have suffered one or more recent significant mergers (e.g. Tormen et al. 1997; Hetzner & Burkert 2006). For this reason, it is common practice to use dynamical state and recent merging history interchangeably, with the understanding implicit that unrelaxed haloes are ones that have suffered one or more recent major mergers.

However, it is important to establish this practice on a more quantitative footing and to assess how well a halo’s dynamical state and its recent mass assembly history correlate. This is because of the need to identify robustly haloes that are in dynamical equilibrium – or indeed disequilibrium – in cosmological simulations<sup>1</sup>. The goal of this paper is to quantify this relationship using a statistical sample of haloes drawn from cosmological  $N$ -body simulations of the CDM model. The CDM model is the ideal testbed for this study because of the fundamental role merging plays in halo mass assembly (e.g. Maulbetsch et al. 2007; Fakhouri & Ma 2008; McBride et al. 2009; Fakhouri & Ma 2010; Fakhouri et al. 2010), and because we expect massive haloes, which on average form later than their less massive counterparts, to have more violent recent merging histories.

Such an undertaking has practical implications. For example, if we want to robustly characterise the predicted variation of, say, concentration  $c_{\text{vir}}$  with virial mass  $M_{\text{vir}}$  on galaxy group and cluster mass scales ( $M_{\text{vir}} \gtrsim 10^{13} M_{\odot}$ ), then it is essential that we can identify relaxed systems in a robust fashion. Should we use mass assembly histories directly and select only haloes that have quiescent recent merging histories, or are commonly used measures that estimate dynamical state based on material within the halo’s virial radius  $r_{\text{vir}}$  adequate? This is particularly important for comparison with observations that provide crucial tests of the theory, such as the analysis the  $M_{\text{vir}} - c_{\text{vir}}$  relation for groups and clusters drawn from the Sloan Digital Sky Survey by Mandelbaum et al. (2008).

In this paper, we examine how a halo’s mass assembly history and dynamical state varies with its virial mass  $M_{\text{vir}}$  and its formation redshift, and adopt simple measures to characterise a halo’s recent mass assembly and merging history – namely, the fraction of mass assembled ( $\Delta M/M$ ); the rate of change of mass with redshift  $1/M dM/dz$ ; and the most significant merger  $\delta_{\text{max}}$ . We compare these with two measures of the halo’s dynamical state – the virial ratio

$$\eta = 2T/|W|, \quad (1)$$

where  $T$  and  $W$  are the kinetic and gravitational potential energies of halo material (cf. Cole & Lacey 1996; Hetzner & Burkert 2006), and the centre-of-mass offset

$$\Delta r = |\vec{r}_{\text{cen}} - \vec{r}_{\text{cm}}|/r_{\text{vir}}, \quad (2)$$

where  $\vec{r}_{\text{cen}}$  and  $\vec{r}_{\text{cm}}$  are the centres of density and mass of halo material and  $r_{\text{vir}}$  is the halo’s virial radius (cf. Crone et al. 1996; Thomas et al. 1998, 2001). Previous studies have shown that both  $\eta$  and  $\Delta r$  increase in the aftermath of a major merger (e.g. Hetzner & Burkert 2006; Poole et al. 2006), and we will clarify

<sup>1</sup> Our focus is fixed firmly on haloes in cosmological simulations, but we note that the relationship between dynamical state and recent mass assembly history is equally important observationally. Here, for example, estimates of the dynamical masses of galaxy clusters require assume a population of dynamical tracers that are in dynamical equilibrium (e.g. Piffaretti & Valdarnini 2008), while reconstructions of a galaxy cluster’s recent merging history look for signatures of disequilibrium (e.g. Cassano et al. 2010). See § 6 for further discussion.

precisely how they relate to a halo’s mass assembly and merging activity in general. We note that our work develops earlier ideas presented in Knebe & Power (2008), in which we investigated the relationship between halo mass  $M_{\text{vir}}$  and spin  $\lambda$ , and it complements that of Davis et al. (2011), who address related but distinct issues in their critique of the application of the virial theorem (cf. §4.1) to simulated high redshift dark matter haloes.

The layout of the paper is as follows. In §2, we describe our approach to making initial conditions; finding and analysing dark matter haloes in evolved outputs; constructing merger trees of our dark matter haloes; and our criteria for defining our halo sample. In §3, we examine the relationship between a halo’s virial mass  $M_{\text{vir}}$ , its formation time  $z_{\text{form}}$  and measures of its mass accretion and merging history. In §4, we present commonly used measures for assessing the dynamical state of a dark matter halo – the virial ratio  $\eta = 2T/|W|$  (cf. §4.1) and the centre-of-mass offset  $\Delta r = |\vec{r}_{\text{cen}} - \vec{r}_{\text{cm}}|/r_{\text{vir}}$  (cf. §4.2) – and investigate how these measures correlate with  $M_{\text{vir}}$  and  $z_{\text{form}}$ . In §5 we combine the insights from the previous two sections and show how a halo’s dynamical state depends on its recent mass accretion and merging history. Finally, we summarise our results in §6 and comment on the implications of our findings for both observational studies and galaxy formation modeling.

## 2 METHODS

### 2.1 The Simulations

We have run a series of  $256^3$  particle cosmological  $N$ -body simulations following the formation and evolution of structure in the CDM model. We use a sequence of boxes of side  $L_{\text{box}}$  varying between  $20h^{-1}\text{Mpc}$  and  $500h^{-1}\text{Mpc}$  from  $z_{\text{start}}=100$  to  $z_{\text{finish}}=0$ . In each case we assume a flat cosmology with a dark energy term, with cosmological parameters  $\Omega_0 = 0.7$ ,  $\Omega_{\Lambda} = 0.3$ ,  $h = 0.7$ , and a normalisation  $\sigma_8 = 0.9$  at  $z = 0$ . Various properties of these simulations are summarised in table 1.

Initial conditions were generated using a standard procedure that can be summarised as follows;

- (i) Generate the CDM transfer function for the appropriate cosmological parameters ( $\Omega_0, \Omega_{\Lambda}, \Omega_b$  and  $h$ ) using the Boltzmann code CMBFAST (Seljak & Zaldarriaga 1996). This is convolved with the primordial power spectrum  $P(k) \propto k^n$ ,  $n = 1$ , to obtain the unnormalised power spectrum, which is normalised by requiring that the linear mass  $\sigma(R)$  equal  $\sigma_8$  on a scale of  $8h^{-1}\text{Mpc}$  at  $z=0$ .
- (ii) Create a statistical realisation of a Gaussian random field of density perturbations in Fourier space, whose variance is given by  $P(k)$ , where  $k = \sqrt{k_x^2 + k_y^2 + k_z^2}$  and whose mean is zero.
- (iii) Take the inverse transform of the density field and compute positions and velocities using the Zel’dovich approximation.
- (iv) Impose these positions and velocities on an initial uniform particle distribution such as a grid or “glass”.

Note that throughout our we use a “glass”-like configuration as our initial uniform particle distribution (White 1996).

All simulations were run using the parallel TreePM code GADGET2 (Springel 2005) with constant comoving gravitational softening  $\epsilon$  and individual and adaptive timesteps for each particle,  $\Delta t = \eta\sqrt{\epsilon/a}$ , where  $a$  is the magnitude of a particle’s gravita-

**Table 1. Properties of the Simulations.** Each of the simulations contains  $256^3$  particles. In addition,  $L_{\text{box}}$  is the comoving box length in units of  $h^{-1}\text{Mpc}$ ;  $N_{\text{run}}$  is the number of runs in the series;  $m_{\text{part}}$  is the particle mass in units of  $h^{-1}M_{\odot}$ ;  $\epsilon$  is the force softening in comoving units of  $h^{-1}\text{kpc}$ ; and  $M_{\text{cut}}$  is the halo mass corresponding to  $N_{\text{cut}}=600$  particles, in units of  $h^{-1}M_{\odot}$ .

Run	$L_{\text{box}}$	$N_{\text{run}}$	$m_{\text{part}}$	$\epsilon$	$M_{\text{cut}}$
$\Lambda\text{CDM}_L20$	20	5	$3.97 \times 10^7$	1.5	$2.38 \times 10^{10}$
$\Lambda\text{CDM}_L50$	50	1	$6.20 \times 10^8$	3.9	$3.72 \times 10^{11}$
$\Lambda\text{CDM}_L70$	70	1	$1.70 \times 10^9$	5.5	$10^{12}$
$\Lambda\text{CDM}_L100$	100	1	$4.96 \times 10^9$	7.8	$2.97 \times 10^{12}$
$\Lambda\text{CDM}_L200$	200	1	$3.97 \times 10^{10}$	15.6	$2.39 \times 10^{13}$
$\Lambda\text{CDM}_L500$	500	1	$6.20 \times 10^{11}$	39.1	$3.72 \times 10^{14}$

tional acceleration and  $\eta = 0.05$  determines the accuracy of the time integration.

## 2.2 Halo Identification and Merger Trees

**Halo Catalogues** Groups were identified using the MPI-enabled version of AHF, otherwise known as AMIGA’s **Halo Finder**<sup>2</sup> (Knollmann & Knebe 2009). AHF is a modification of MHF (MLAPM’s Halo Finder; see Gill et al. 2004) that locates groups as peaks in an adaptively smoothed density field using a hierarchy of grids and a refinement criterion that is comparable to the force resolution of the simulation. Local potential minima are calculated for each of these peaks and the set of particles that are gravitationally bound to the peaks are identified as groups that form our halo catalogue.

For each halo in the catalogue we determine its centre-of-density  $\vec{r}_{\text{cen}}$  (using the iterative “shrinking spheres” method described in Power et al. 2003) and identify this as the halo centre. From this, we calculate the halo’s virial radius  $r_{\text{vir}}$ , which we define as the radius at which the mean interior density is  $\Delta_{\text{vir}}$  times the critical density of the Universe at that redshift,  $\rho_c(z) = 3H^2(z)/8\pi G$ , where  $H(z)$  and  $G$  are the Hubble parameter at  $z$  and the gravitational constant respectively. The corresponding virial mass  $M_{\text{vir}}$  is

$$M_{\text{vir}} = \frac{4\pi}{3} \Delta_{\text{vir}} \rho_c r_{\text{vir}}^3. \quad (3)$$

We adopt a cosmology- and redshift-dependent overdensity criterion, which for a  $\Lambda\text{CDM}$  cosmology with  $\Omega_0 = 0.3$  and  $\Omega_{\Lambda} = 0.7$  gives  $\Delta_{\text{vir}} \simeq 97$  at  $z=0$  (c.f. Eke et al. 1998).

**Merger Trees** Halo merger trees are constructed by linking halo particles at consecutive output times;

- For each pair of group catalogues constructed at consecutive output times  $t_1$  and  $t_2 > t_1$ , the “ancestors” of “descendent” groups are identified. For each descendent identified in the catalogue at the later time  $t_2$ , we sweep over its associated particles and locate every ancestor at the earlier time  $t_1$  that contains a subset of these particles. A record of all ancestors at  $t_1$  that contain particles associated with the descendent at  $t_2$  is maintained.

- The ancestor at time  $t_1$  that contains in excess of  $f_{\text{prog}}$  of these particles and also contains the most bound particle of the descendent at  $t_2$  is deemed the *main progenitor*. Typically  $f_{\text{prog}} = 0.5$ , i.e. the main progenitor contains in excess of half the final mass.

Each group is then treated as a node in a tree structure, which can be traversed either forwards, allowing one to identify a halo at some early time and follow it forward through the merging hierarchy, or backwards, allowing one to identify a halo and all its progenitors at earlier times.

## 2.3 Defining the Halo Sample

A degree of care must be taken when choosing which haloes to include in our sample, to ensure that our results are not affected by the finite resolution of our simulations. One of the key calculations in this study is of a halo’s virial ratio  $\eta = 2T/|W|$  (see § 4.1), where  $T$  and  $W$  are the kinetic and gravitational potential energies of material within  $r_{\text{vir}}$ . The gravitational potential energy is particularly sensitive to resolution; if a halo is resolved with too few particles, its internal structure will not be recovered sufficiently accurately and the magnitude of  $W$  will be underestimated.

We estimate how many particles are needed to recover  $W$  robustly from a  $N$ -body simulation in Figure 1. Here we generate Monte Carlo  $N$ -body realisations of a halo whose spherically averaged mass profile is described by the Navarro et al. (1997) profile,

$$\frac{\rho(x)}{\rho_c} = \frac{\delta_c}{cx(1+cx)^2}; \quad (4)$$

here  $x = r/r_{\text{vir}}$  is the radius  $r$  normalised to  $r_{\text{vir}}$ ,  $c$  is the concentration parameter and  $\delta_c$  is the characteristic density,

$$\delta_c = \frac{\Delta_{\text{vir}}}{3} \frac{c^3}{\ln(1+c) - c/(1+c)}. \quad (5)$$

The resulting gravitational potential energy is given by

$$W = -16\pi^2 G \rho_c^2 \delta_c^2 \left(\frac{r_{\text{vir}}}{c}\right)^5 \times \left[ \frac{c}{2} \frac{(2+c)}{(1+c)^2} - \frac{\ln(1+c)}{(1+c)} \right]. \quad (6)$$

In a  $N$ -body simulation or realisation, we calculate  $W$  by randomly sampling particles within  $r_{\text{vir}}$  and rescaling; this gives

$$W = \left( \frac{N_{\text{vir}}^2 - N_k}{N_k^2 - N_k} \right) \left( \frac{-Gm_p^2}{\epsilon} \right) \sum_i^{N_k-1} \sum_{j=i+1}^{N_k} -K_s(|r_{ij}|/\epsilon), \quad (7)$$

where there are  $N_{\text{vir}}$  particles in the halo, each of mass  $m_p$ . We sample  $N_k$  particles from  $N_{\text{vir}}$ ,  $|r_{ij}|$  is the magnitude of the separation between particles  $i$  at  $\vec{r}_i$  and  $j$  at  $\vec{r}_j$ , and the prefactor  $(N^2 - N)/(N_k^2 - N_k)$  accounts for particle sampling.  $\epsilon$  is the gravitational softening and  $K_s$  corresponds to the softening kernel used in GADGET2. For the Monte Carlo realisations in Figure 1 we set  $\epsilon$  to be vanishingly small, but for the simulations we use  $\epsilon$  as it is listed in table 1.

Figure 1 shows  $|W|$  measured for Monte Carlo realisations of a halo with  $c=10$  and  $r_{\text{vir}}=200$  kpc as a function of  $N_{\text{vir}}$ . For comparison the horizontal dotted lines indicate the value of  $|W|$  ( $\pm 5\%$ ) we expect from equation (6). If  $N_{\text{vir}} \approx 300$  or fewer, the measured  $|W|$  deviates from the expected  $|W|$  by greater than 5%; therefore we might regard  $N_{\text{cut}} = 300$  as the lower limit on  $N_{\text{vir}}$  for a halo to be included in our sample. However, we adopt a more conservative  $N_{\text{cut}} = 600$  in the remainder of this paper; this is because the structure of simulated haloes are affected by finite gravitational softening (cf. Power et al. 2003), they are seldom (if ever) smooth and spherically symmetric (e.g. Bailin & Steinmetz

<sup>2</sup> AHF may be downloaded from <http://popia.ft.uam.es/AMIGA>

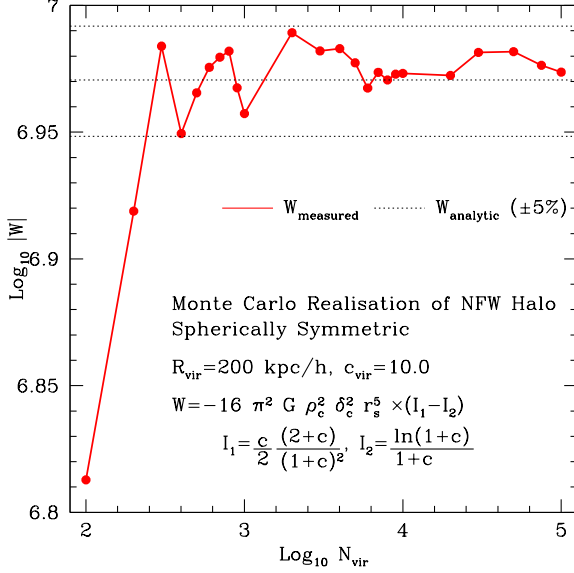


**Figure 1.** How many particles are required to measure accurately the gravitational binding energy of a dark matter halo? Here we generate Monte Carlo realisations of a NFW halo and calculate the gravitational potential energy of material within the virial radius. If there are too few particles within  $r_{\text{vir}}$ , the potential energy will be inaccurate.

2005), as we assumed in our simple calculation, and there can be a range of concentrations at a given mass (Bullock et al. 2001), which will affect any estimate of  $W$  as inspection of equation (6) reveals.

### 3 QUANTIFYING MASS ASSEMBLY & MERGING HISTORY

In this section we establish quantitative measures for a halo’s mass accretion and merging histories, and we examine how these measures relate to virial mass  $M_{\text{vir}}$  and formation redshift  $z_{\text{form}}$ .

**Quantifying Formation Redshift** We begin our analysis by verifying the correlation between virial mass  $M_{\text{vir}}$  and formation redshift  $z_{\text{form}}$  for our halo sample. We adopt the convention of Cole & Lacey (1996) and define  $z_{\text{form}}$  as the redshift at which the mass of the main progenitor of a halo of mass  $M_{\text{vir}}(z)$  identified at  $z$  first exceeds  $M_{\text{vir}}(z)/2$ . This is equivalent to  $z_{1/2,\text{mb}}$  in the survey of halo formation redshift definitions examined by Li et al. (2008).

Our expectation is that more massive CDM haloes will assemble more of their mass at later times than their lower mass counterparts and this is borne out by Figure 2. Here we show the variation of  $z_{\text{form}}$  with  $M_{\text{vir}}$  for our halo sample; the filled circles and bars indicate the medians and upper and lower quartiles respectively, within logarithmic mass bins of width 0.5 dex. The relationship between the mean and median  $z_{\text{form}}$  with  $M_{\text{vir}}$  can be well approximated by

$$\langle z_{\text{form}} \rangle \simeq -0.22 \log_{10} M_{12} + 1.06, \quad (8)$$

and

$$\text{Med } z_{\text{form}} \simeq -0.23 \log_{10} M_{12} + 1.08, \quad (9)$$

where  $M_{12}$  is  $M_{\text{vir}}$  in units of  $10^{12} h^{-1} M_{\odot}$ . This is in very good

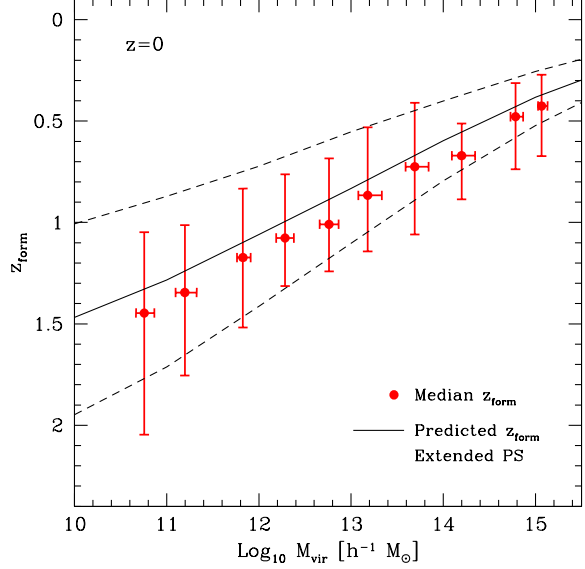


**Figure 2.** Relationship between Virial Mass and Formation Redshift.

Here we show how the formation redshift  $z_{\text{form}}$  varies with virial mass  $M_{\text{vir}}$  at  $z=0$ . We determine  $z_{\text{form}}$  directly from a halo’s merger tree – for a halo of  $M_{\text{vir}}$  identified at  $z=0$ , we identify the redshift  $z_{\text{form}}$  at which the mass of its main progenitor first exceeds half its virial mass at  $z=0$ . Data are binned using equally spaced bins in  $\text{Log}_{10} M_{\text{vir}}$ ; filled circle and bars correspond to medians, upper and lower quartiles. The solid, upper and lower dashed curves corresponds to the median  $z_{\text{form}}$  and its upper and lower quartiles predicted by extended Press-Schechter theory (cf. Lacey & Cole 1993).

agreement with the mean variation reported for the “Overall” sample of haloes drawn from the Millennium and Millennium II simulations (cf. Springel et al. 2005 and Boylan-Kolchin et al. 2009 respectively) in Table 3 of McBride et al. (2009), who found

$$\langle z_{\text{form}} \rangle = -0.24 \log_{10} M_{12} + 1.26.$$

We show also the variation predicted by extended Press-Schechter (EPS) theory for our choice of CDM power spectrum – see the solid and dashed curves, indicating the median, upper and lower quartiles of the distributions (cf. Lacey & Cole 1993). These curves were generated using realisations of  $10^6$  Monte-Carlo merger trees for haloes with  $z=0$  masses in the range  $10^{10} \leq M_{\text{vir}}/h^{-1} M_{\odot} \leq 10^{15.5}$ . We note a slight but systematic offset between the medians evaluated from the simulated haloes and those predicted by EPS theory, such that the simulated haloes tend to form earlier than predicted. This effect has been reported previously by both van den Bosch (2002) and Maubetsch et al. (2007).

**Quantifying Recent Mass Accretion History** Because more massive systems tend to form later than their less massive counterparts, it follows that the rate at which a halo assembles its mass should increase with increasing  $M_{\text{vir}}$  and decreasing  $z_{\text{form}}$ . The recent comprehensive study by McBride et al. (2009) provides a useful fitting formula that captures the complexity of a halo’s mass accretion history and allows haloes to be categorised into different Types I to IV, which depend on their growth rates. However, we adopt two simple well-defined measures of a halo’s mass accretion rate that have a straightforward interpretation;

- $(\Delta M/M)_{\Delta t}$ , the fraction of mass that has been accreted by a halo during a time interval  $\Delta t$ ; and
- $\alpha = 1/M dM/dz$ , the rate of fractional change in a halo's virial mass with respect to redshift over a redshift interval  $\Delta z$ .

Note that  $\alpha$  is equivalent to the  $\alpha$  free parameter used in Wechsler et al. (2002). We find that  $(\Delta M/M)_{\Delta t}$  and  $\alpha$  are sufficient as simple measures of the mass accretion rate and we use them in the remainder of this paper.

For the fiducial timescale  $\Delta t$ , we use twice the dynamical timescale  $\tau_{\text{dyn}}$  estimated at the virial radius,

$$\tau_{\text{dyn}} = \sqrt{2} \frac{r_{\text{vir}}}{V_{\text{vir}}} = 2.8 \left( \frac{\Delta_{\text{vir}}}{97} \right)^{-1/2} \left( \frac{H(z)}{70} \right)^{-1} \text{ Gyrs} \quad (10)$$

Note that  $\tau_{\text{dyn}}$  depends only on  $z$  and is the same for all haloes. For our adopted cosmological parameters,  $\Delta(z) \simeq 97$  at  $z=0$ , and so  $\Delta t = 2\tau_{\text{dyn}} \simeq 5.6$  Gyr which corresponds to a redshift interval of  $\Delta z \simeq 0.6$  at  $z=0$ . Merging proceeds on a timescale  $\tau_{\text{merge}} \gtrsim \tau_{\text{dyn}}$ , with  $\tau_{\text{merge}} \rightarrow \tau_{\text{dyn}}$  as the mass ratio of the merger decreases. Our adopted timescale of  $\Delta t = 2\tau_{\text{dyn}}$  for the response of a halo to a merger is reasonable when compared to typical values of  $\tau_{\text{merge}}/\tau_{\text{dyn}}$  expected for haloes in cosmological simulations, as estimated by Boylan-Kolchin et al. (2008)<sup>3</sup>.

We determine both  $(\Delta M/M)_{\tau_{\text{dyn}}}$  and  $\alpha$  directly from each halo's merger tree by tracking  $M_{\text{vir}}(z)$  of its main progenitor over the interval  $\Delta z$ ;  $\alpha$  is obtained by taking the natural logarithm of the progenitor mass at each redshift and estimating its value by linear regression. Haloes that have high mass accretion rates will have  $(\Delta M/M)_{\Delta t} \rightarrow 1$  and  $\alpha \rightarrow -\infty$ .

In Fig. 3 we show how a halo's mass accretion rate correlates with its virial mass and formation time.  $(\Delta M/M)_{\tau_{\text{dyn}}}$  ( $\alpha$ ) shows a steady monotonic increase (decrease) as  $M_{\text{vir}}$  increases over the range  $10^{10} h^{-1} M_{\odot} \lesssim M_{\text{vir}} \lesssim 10^{15} h^{-1} M_{\odot}$ . For example, inspection of  $(\Delta M/M)_{\tau_{\text{dyn}}}$  reveals that  $\lesssim 15\%$  of the virial mass of a halo with  $M_{\text{vir}} \sim 10^{12} h^{-1} M_{\odot}$  has been accreted since  $z \simeq 0.5$ , compared to  $\sim 50\%$  for haloes with  $M_{\text{vir}} \sim 10^{15} h^{-1} M_{\odot}$  over the same period.  $(\Delta M/M)_{\tau_{\text{dyn}}}$  ( $\alpha$ ) shows a similar increase (decrease) with decreasing  $z_{\text{form}}$  although it's interesting to note that the trend flattens off for haloes that form at  $z \gtrsim 2$ .

This analysis confirms our theoretical prejudice that more massive haloes and haloes that formed more recently tend to be the haloes with the measurably highest accretion rates. Reassuringly, our results are in good agreement with the findings of recent studies. For example, McBride et al. (2009) examined the mass accretion and merging histories of a much larger sample of haloes drawn from the Millennium and Millennium-II simulations and found that the mean instantaneous mass accretion rate varies with halo mass as  $\dot{M}/M \propto M^{0.127}$ ; this compares favourably with our equivalent measure,  $(\Delta M/M)_{\tau_{\text{dyn}}} \propto M_{\text{vir}}^{0.14}$ . Maulbetsch et al. (2007) looked at halo accretion rates, normalised to their maximum masses, over the redshift interval  $z=0.1$  to 0 for haloes with masses  $10^{11} \leq M_{\text{vir}}/h^{-1} M_{\odot} \leq 10^{13}$  and found only a weak dependence on halo mass, with higher mass haloes have higher rates. This is consistent with our results for  $\alpha$ , whose median value changes by  $\sim 10\%$  over the same range in halo mass.

<sup>3</sup> In particular, we refer to their equation 5 with values of  $j/j_{\text{C}}(E) = 0.5$  and  $r_{\text{C}}(E)/r_{\text{vir}}$  that are consistent with the results of cosmological simulations. Here  $j$  is the specific angular momentum of a merging subhalo,  $j_{\text{C}}(E)$  is the specific angular momentum of the circular orbit corresponding to the subhalo's orbital energy  $E$ , and  $r_{\text{C}}(E)$  is the radius corresponding to this circular orbit.

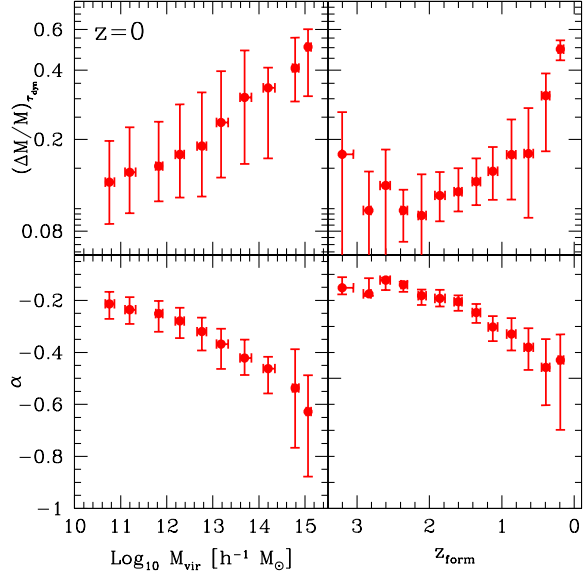


**Figure 3. Relationship between Recent Mass Accretion History, Halo Mass and Formation Redshift.** For each halo of virial mass  $M_{\text{vir}}$  and formation redshift  $z_{\text{form}}$  identified at  $z=0$ , we follow its merger tree back for one dynamical time  $\tau_{\text{dyn}}$  ( $\simeq 4.6$  Gyrs,  $\Delta z \simeq 0.45$ ) and characterise its mass accretion history using two measures. The first is  $(\Delta M/M)_{\tau_{\text{dyn}}}$ , the fraction of mass accreted over  $\tau_{\text{dyn}}$  (upper panels), and the second is  $\alpha$ , the average mass accretion rate of Wechsler et al. (2002) (lower panels). Data points and bars correspond to medians and upper and lower quartiles. Note that we use equally-spaced logarithmic bins in  $M_{\text{vir}}$  and  $z_{\text{form}}$ .

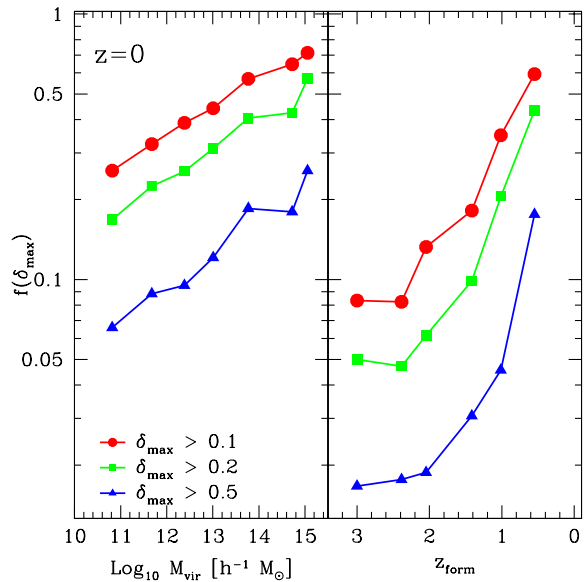


**Figure 4. Frequency of Major Mergers and Dependence on Halo Mass and Formation Redshift.** Here we determine the most significant merger of mass ratio  $\delta_{\text{max}} = M_{\text{acc}}(z_i)/M_{\text{vir}}(z_f)$  experienced by each halo since  $z=0.5$ , where  $z_i$  and  $z_f$  correspond to the initial and final redshifts. We then compute the fraction of haloes  $f(\delta_{\text{max}})$  at a given virial mass (left hand panel) and given formation redshift (right hand panel) that have experienced mergers with mass ratios  $\delta_{\text{max}}$  in excess of 10% (filled circles), 20% (filled squares) and 50% (filled triangles).

**Quantifying Recent Merger Activity** Both  $(\Delta M/M)_{\tau_{\text{dyn}}}$  and  $\alpha$  provide useful insights into a halo’s total mass accretion rate, but they cannot distinguish between smooth and clumpy accretion. In Fig. 4 we focus specifically on a halo’s merger history by considering the likelihood that a halo of a given  $M_{\text{vir}}$  (left hand panel) or  $z_{\text{form}}$  (right hand panel) has experienced *at least one* merger with a mass ratio  $\delta_{\text{max}}$  since  $z=0.6$ .

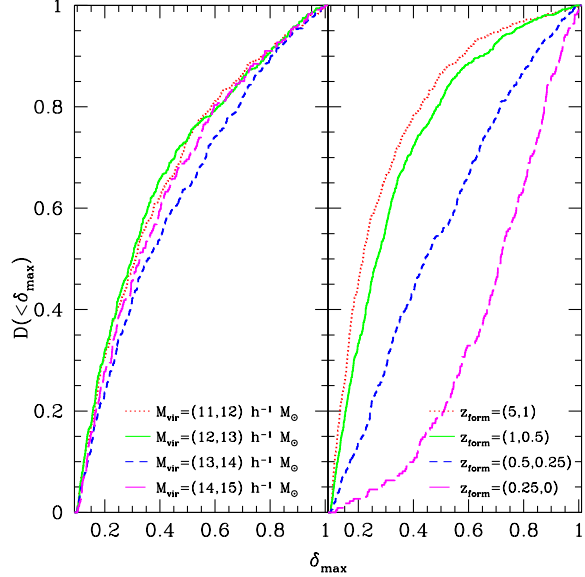
Each halo identified at  $z=0$  has a unique merger history, which characterises not only how its  $M_{\text{vir}}$  grows as a function of time but also details of mergers it has experienced over time. Using this merger history, we construct the distribution of mass ratios of mergers  $\delta$  experienced by a halo of a given  $M_{\text{vir}}$  or  $z_{\text{form}}$  between  $0 \leq z \lesssim 0.6$ . We define  $\delta = M_{\text{acc}}(z_i, z_f)/M_{\text{vir}}(z_f)$  where  $M_{\text{acc}}(z_i, z_f)$  is the mass of the less massive halo prior to its merging with the more massive halo,  $M_{\text{vir}}(z_f)$  is the virial mass of the more massive halo once the less massive halo has merged with it, and  $z_i > z_f$  and  $z_f$  are the redshifts of consecutive simulation snapshots. The maximum value of  $\delta$  for a given halo gives us its  $\delta_{\text{max}}$  and we use this to compute the fraction of haloes of a given  $M_{\text{vir}}$  or  $z_{\text{form}}$  that have  $\delta_{\text{max}}$  in excess of 10% (filled circles), 20% (filled squares) and 50% (filled triangles).

Fig. 4 reveals that mergers with higher mass ratios (i.e. minor mergers) are more common than mergers with lower mass ratios (i.e. major mergers), independent of  $M_{\text{vir}}$  and  $z_{\text{form}}$ , and that more massive (older) haloes tend to experience more mergers than their lower mass (younger) counterparts. For example, the likelihood that a  $10^{12} h^{-1} M_{\odot}$  galaxy-mass halo experiences a merger with  $\delta_{\text{max}} > 10\%$  is  $\sim 35\%$ , compared to 25%(10%) for  $\delta_{\text{max}} > 20\%$ (50%). In contrast, the likelihood that a  $10^{14} h^{-1} M_{\odot}$  cluster-mass halo experiences mergers with  $\delta_{\text{max}} > 10\%$ (20%, 50%) is  $\sim 60\%$ (40%, 20%). Interestingly, we find that the fraction of haloes that have experienced a merger more significant than  $\delta_{\text{max}}$  increases with  $M_{\text{vir}}$  approximately as  $f(\delta_{\text{max}}) \propto M_{\text{vir}}^{0.11}$ .

These results are broadly in agreement with the findings of Fakhouri et al. (2010). Inspection of the leftmost panel of their Figure 7 shows the mean number of mergers with mass ratios greater than 1:10 and 1:3 between  $z=0$  and  $z \sim 0.6$  increases with increasing halo mass, such that a  $10^{12} (10^{14}) h^{-1} M_{\odot}$  has a likelihood of  $\sim 40\%$  ( $\sim 80\%$ ) to have experienced a merger with  $\delta_{\text{max}} > 10\%$ , and a likelihood of  $\sim 20\%$  ( $\sim 40\%$ ) to have experienced a merger with  $\delta_{\text{max}} > 33\%$ .

In Fig. 5 we show the full (cumulative) distributions of  $\delta_{\text{max}}$  for haloes split into bins according to  $M_{\text{vir}}$  (left hand panel) and  $z_{\text{form}}$  (right hand panel); note that we consider only haloes with  $\delta_{\text{max}} \geq 10\%$ . Interestingly this figure reveals that the probability distribution of  $\delta_{\text{max}}$  is insensitive to  $M_{\text{vir}}$ , but depends strongly on  $z_{\text{form}}$ . For example, the median  $\delta_{\text{max,med}} \simeq 0.3$ , independent of  $M_{\text{vir}}$  whereas it increases from  $\delta_{\text{max,med}} \simeq 0.2$  for haloes with  $z_{\text{form}} \gtrsim 0.5$  to  $\delta_{\text{max,med}} \simeq 0.4$  for haloes with  $0.25 \leq z_{\text{form}} \leq 0.5$  and  $\delta_{\text{max,med}} \simeq 0.7$  for haloes with  $0 \leq z_{\text{form}} \leq 0.25$ .

Figs. 3 to 5 demonstrate that there is a strong correlation at  $z=0$  between a halo’s virial mass  $M_{\text{vir}}$ , its formation redshift  $z_{\text{form}}$  and the rate at which it has assembled its mass through accretion and merging over the last  $\tau_{\text{dyn}}$  or equivalently  $\Delta z \sim 0.6$ . We use these results in §5, where we investigate the degree to which a halo’s  $M_{\text{vir}}$ ,  $z_{\text{form}}$  and mass accretion rate affect the degree to which it is in dynamical equilibrium.



**Figure 5. Cumulative Distribution of  $\delta_{\text{max}}$  as a Function of Halo Mass and Formation Redshift.** We show how the fraction of haloes whose most significant merger’s mass ratio is less than  $\delta_{\text{max}}$ , as a function of virial mass (left hand panel) and formation redshift (right hand panel). Note that we select only haloes that have  $\delta_{\text{max}} \geq 10\%$ , and we consider only mergers between  $z=0.5$  and  $z=0$ . In the key, the numbers in brackets correspond to the lower and upper bounds in  $M_{\text{vir}}$  and  $z_{\text{form}}$ .

## 4 QUANTIFYING DYNAMICAL EQUILIBRIUM

In this section we describe the two commonly used quantitative measures for a halo’s dynamical state, the virial ratio  $\eta$  and the centre of mass offset  $\Delta r$ , and we examine their relationship with virial mass  $M_{\text{vir}}$  and formation redshift  $z_{\text{form}}$ .

### 4.1 The Virial Ratio $\eta$

The virial ratio  $\eta$  is commonly used in cosmological  $N$ -body simulations as a measure of a halo’s dynamical state (e.g. Cole & Lacey 1996; Bett et al. 2007; Neto et al. 2007; Knebe & Power 2008; Davis et al. 2011). It derives from the virial theorem,

$$\frac{1}{2} \frac{d^2 I}{dt^2} = 2T + W + E_S, \quad (11)$$

where  $I$  is the moment of inertia,  $T$  is the kinetic energy,  $W = \Sigma \vec{F} \cdot \vec{r}$  is the virial, and  $E_S$  is the surface pressure integrated over the bounding surface of the volume within which  $I$ ,  $T$  and  $W$  are evaluated (cf. Chandrasekhar 1961). Provided the system is isolated and bounded, the virial  $W$  is equivalent to the gravitational potential energy. While not strictly true for haloes that form in cosmological  $N$ -body simulations, the convention has been to evaluate  $W$  as the gravitational potential energy with this caveat in mind (e.g. Cole & Lacey 1996). We follow this convention and treat  $W$  as the gravitational potential energy computed using equation (7).

If the system is in a steady state and in the absence of surface pressure, equation (11) reduces to  $2T + W = 0$ , which can be written more compactly as  $2T/|W| = 1$  (e.g. Cole & Lacey 1996). We refer to the ratio  $\eta = 2T/|W|$  as the virial ratio and we expect  $\eta \rightarrow 1$  for dynamically relaxed haloes. However, we might expect  $E_S$  to be important for haloes that form in cosmological



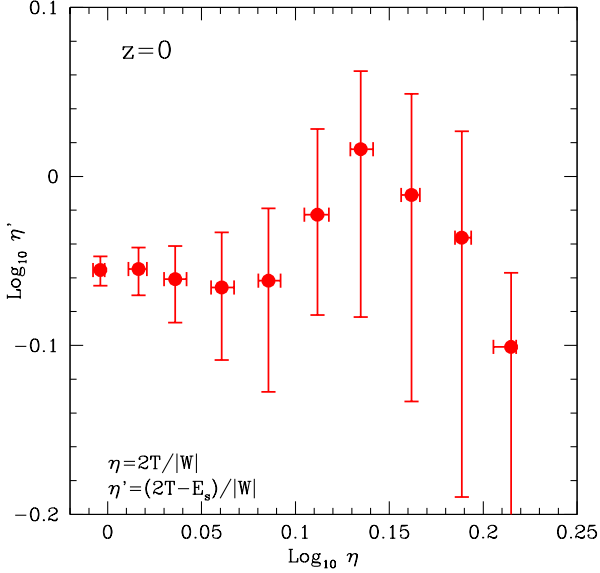


**Figure 6. Correlation between Virial Ratios  $\eta$  and  $\eta'$ .** We bin all haloes in our sample at  $z=0$  according to their  $\eta$  and evaluate the median  $\eta'$  within each bin. The upper and lower quartiles of the distributions in  $\eta$  and  $\eta'$  are indicated by bars.

$N$ -body simulations; in this case Shaw et al. (2006) have proposed modifying the virial ratio to obtain

$$\eta' = (2T - E_s)/|W|. \quad (12)$$

We calculate both  $T$  and  $W$  using all material within  $r_{\text{vir}}$ , while we follow Shaw et al. (2006) by computing the surface pressure contribution from all particles that lie in a spherical shell with inner and outer radii of 0.8 and 1.0  $r_{\text{vir}}$ ,

$$P_s = \frac{1}{3V} \sum_i (m_i v_i^2); \quad (13)$$

here  $V$  corresponds to the volume of this shell and  $v_i$  are the particle velocities relative to the centre of mass velocity of the halo. The energy associated with the surface pressure is therefore  $E_s \simeq 4\pi r_{\text{med}}^3 P_s$  where  $r_{\text{med}}$  is the median radius of the shell.

Figure 6 shows how the median  $\eta$  and  $\eta'$  for the haloes in our sample compare, with bars indicating the upper and lower quartiles of the distributions. We might expect that  $\eta' \sim 1$  and insensitive to variation in  $\eta$ ; however, this figure reveals that the relationship between  $\eta$  and  $\eta'$  is not so straightforward. Haloes that we would expect to be dynamically relaxed, with  $\eta \sim 1$ , have values of  $\eta' < 0$ , suggesting that  $E_s$  tends to over-correct. Similar behaviour has been noted in both Knebe & Power (2008) and Davis et al. (2011) for high redshift haloes ( $z \gtrsim 1$ ). The relation between the median  $\eta$  and  $\eta'$  is flat  $\eta \lesssim 1.25$  but rises sharply from  $\eta' \sim 0.9$  to peak at  $\eta' \sim 1.05$  before declining sharply for  $\eta \gtrsim 1.4$  to a median of  $\eta' \sim 0.8$  in the last plotted bin. Interestingly, the width of the  $\eta'$  distribution increases with  $\eta$ ; if  $\eta$  tracks recent major merging activity as we expect, then this suggests that  $\eta'$  – and consequently the surface pressure correction term  $E_s$  – is sensitive to mergers but in a non-trivial way.

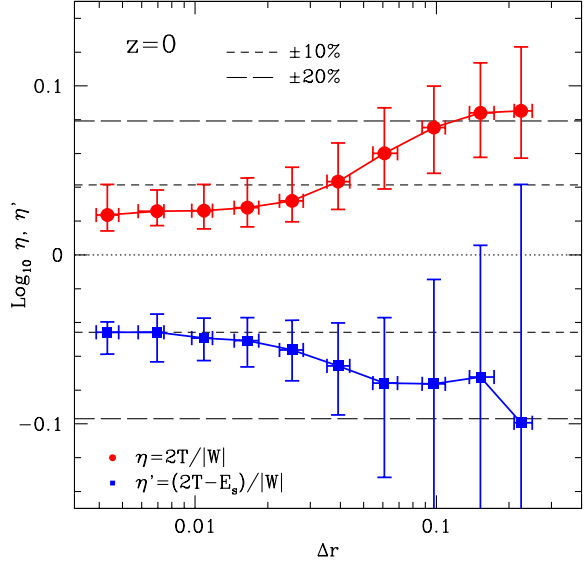


**Figure 7. Correlation between Centre-of-Mass Offset  $\Delta r$  and Virial Ratios  $\eta$  and  $\eta'$ .** We can clearly see the relation which is confirmed by measuring a Spearman rank coefficient of 0.45 whereas we find an anti-correlation with Spearman rank coefficient of -0.18 for  $\eta'$ .

## 4.2 The Centre-of-Mass Offset $\Delta r$

Another commonly used measure of a halo's dynamical state is the centre-of-mass offset  $\Delta r$ ,

$$\Delta r = \frac{|\vec{r}_{\text{cen}} - \vec{r}_{\text{cm}}|}{r_{\text{vir}}}, \quad (14)$$

which measures the separation between a halo's centre-of-density  $\vec{r}_{\text{cen}}$  (calculated as described in §2.2) and its centre-of-mass, calculated using all material within  $r_{\text{vir}}$ , normalised by  $r_{\text{vir}}$  (cf. Crone et al. 1996; Thomas et al. 1998, 2001; Neto et al. 2007; Macciò et al. 2007; D'Onghia & Navarro 2007).  $\Delta r$  is used as a substructure statistic, providing an estimate of a halo's deviations from smoothness and spherical symmetry. The expectation is that the smaller the  $\Delta r$ , the more relaxed the halo; for example, Neto et al. (2007) define dynamically relaxed haloes to be those with  $\Delta r \leq 0.07$ , while D'Onghia & Navarro (2007) adopt  $\Delta r \leq 0.1$ . Macciò et al. (2007) favoured a more conservative  $\Delta r \leq 0.04$  based on a thorough analysis.

We can get a sense of how well  $\Delta r$  measures the dynamical state of a halo by comparing it to  $\eta$  and  $\eta'$ . In Figure 7 we plot the median  $\eta$  and  $\eta'$  (filled circles and squares respectively) against the median  $\Delta r$ ; as before, bars indicate the upper and lower quartiles of the distributions. This figure shows that both  $\eta$  and  $\eta'$  correlate with  $\Delta r$  – but in different senses; as  $\Delta r$  increases,  $\eta$  increases while  $\eta'$  decreases. The increase (decrease) is a gradual one; for example, for  $\Delta r \lesssim 0.04$ , the median  $\eta$  is flat with a value of  $\sim 1.05$ , but for  $\Delta r \gtrsim 0.04$  there is a sharp increase and  $\Delta r \gtrsim 0.1$ ,  $\eta \sim 1.2$ . Although direct comparison is difficult, a similar trend can be gleaned from Figure 2 of Neto et al. (2007). We use the Spearman rank correlation coefficient to assess the strength of the correlation between  $\Delta r$  and  $\eta(\eta')$  (cf. Kendall & Gibbons 1990), and find strong positive and negative correlations for  $\eta$  (Spearman rank coefficient  $r=0.97$ ) and  $\eta'$  ( $r=-0.95$ ) respectively.

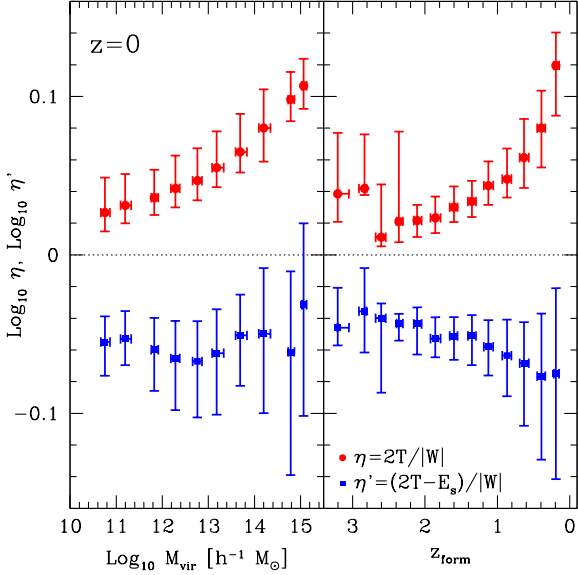


**Figure 8. Relationship between Dynamical State and Halo Mass and Formation Redshift.** For haloes identified at  $z=0$ , we plot the median  $\eta$  and  $\eta'$  versus  $M_{\text{vir}}$  (left hand panel) and  $z_{\text{form}}$  (right hand panel) using equally spaced bins in  $\text{Log}_{10} M_{\text{vir}}$  and  $z_{\text{form}}$ . Data points and bars correspond to medians and upper and lower quartiles.

This is suggestive – as we show below,  $\Delta r$  correlates more strongly with merging activity than either of  $\eta$  or  $\eta'$  (cf. Figure 13 in §5). Both  $\Delta r$  and  $\eta$  increase with strength of merging activity, whereas  $\eta'$  appears to be over-corrected by  $E_s$  (as we have noted above). From this we conclude that  $E_s$  (as we evaluate it) correlates with significant merger activity, which is confirmed by a Spearman rank coefficient of 0.38 for the correlation between  $E_s$  and  $\delta_{\text{max}}$ .

Interestingly Davis et al. (2011) examined the correlation between  $\Delta r$  and  $\eta'$  for high redshift haloes ( $z \gtrsim 6$ ) and noted a tendency for haloes with small values of  $\eta'$  to have larger values of  $\Delta r$ . Inspection of their Figure 4 shows that this is true for haloes with  $0.4 \lesssim \Delta r \lesssim 10$ ; for  $\Delta r \lesssim 0.4$  the relation with  $\eta'$  is flat. Davis et al. (2011) argue that, because there is no systematic shift in  $\eta'$  for  $\Delta r < 0.1$ ,  $\Delta r$  is not a useful measure of dynamical state at high redshifts.

#### 4.3 Dependence of Dynamical State on $M_{\text{vir}}$ and $z_{\text{form}}$

In Figures 8 and 9 we examine how  $\eta$ ,  $\eta'$  and  $\Delta r$  vary with  $M_{\text{vir}}$  (left hand panels) and  $z_{\text{form}}$  (right hand panels) for the halo population at  $z=0$ . Haloes are sorted in bins of equal width in mass ( $\Delta \log_{10} M = 0.5$  dex) and redshift ( $\Delta z = 0.25$ ), and we plot the median  $\eta/\eta'/\Delta r$  within each bin against the median  $M_{\text{vir}}/z_{\text{form}}$ ; bars indicate the upper and lower quartiles of the respective distributions. For reference, we also plot a horizontal dotted line in each panel of Figure 8 to indicate a virial ratio of unity.

Because more massive haloes tend to form at later times, and because these haloes tend to assemble a larger fraction of their mass more recently, we expect that  $\eta$  and  $\Delta r$  should increase with increasing  $M_{\text{vir}}$  and decreasing  $z_{\text{form}}$ . This is borne out in Figures 8 and 9. We find that the mean and median  $\Delta r$  increases steadily with increasing  $M_{\text{vir}}$  as

$$\langle \log_{10} \Delta r \rangle = -1.47 + 0.08 \log_{10} M_{12} \quad (15)$$

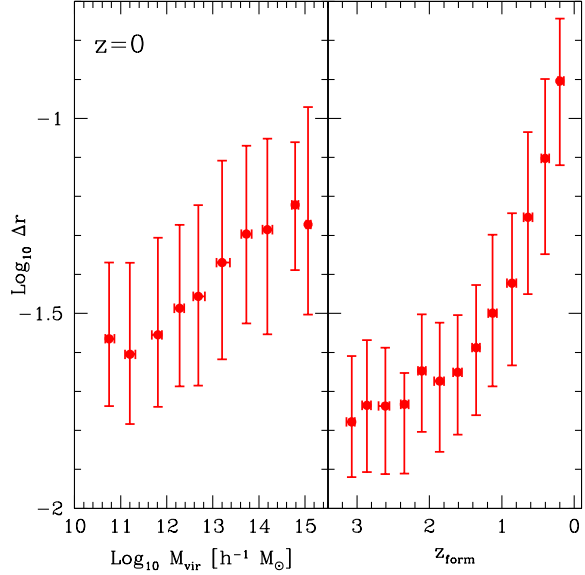


**Figure 9. Relationship between Centre-of-Mass Offset, Halo Mass and Formation Redshift.** For haloes identified at  $z=0$ , we plot the median centre-of-mass offset  $\Delta r$  versus  $M_{\text{vir}}$  (left hand panel) and  $z_{\text{form}}$  (right hand panel) using equally spaced bins in  $\text{Log}_{10} M_{\text{vir}}$  and  $z_{\text{form}}$ . Data points and bars correspond to medians and upper and lower quartiles.

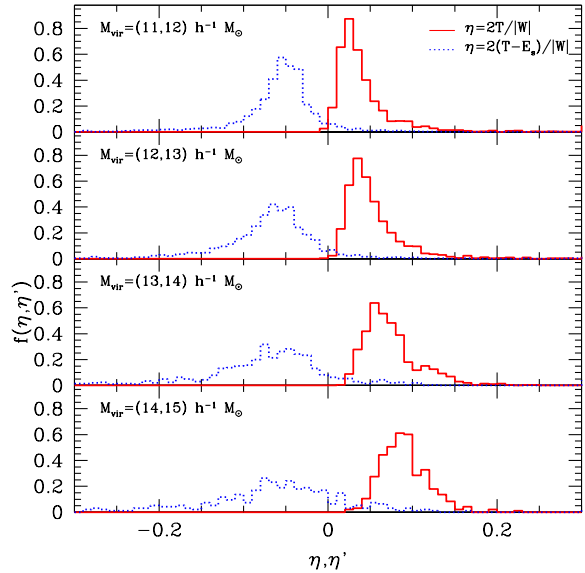


**Figure 10. Distribution of virial ratios.** Here we show the correlation between halo mass and virial ratio  $\eta$  and  $\eta'$  at redshift  $z = 0$ .

and

$$\text{Med } \log_{10} \Delta r = -1.49 + 0.09 \log_{10} M_{12} \quad (16)$$

where, as before,  $M_{12}$  is  $M_{\text{vir}}$  in units of  $10^{12} h^{-1} M_{\odot}$ . This is consistent with the result of Thomas et al. (2001, see their Figure 9), who found a similar trend for  $\Delta r$  to increase with  $M_{180}$  for a sample of cluster mass haloes ( $10^{13} \lesssim M_{180}/(h^{-1} M_{\odot}) \lesssim 10^{15}$ ) in a  $\tau$ CDM model. Their typical values of  $\Delta r$  are offset to higher values than we find, but this can be understood as an effect of  $\Lambda$ ,



the merging rate being suppressed in the  $\Lambda$ CDM model compared to the  $\tau$ CDM model. Similarly,  $\Delta r$  varies strongly with  $z_{\text{form}}$ ; for  $z_{\text{form}} \gtrsim 1$  we find that  $\Delta r \propto (1+z)^{-0.65}$  compared to  $\Delta r \propto (1+z)^{-0.1}$  for  $z_{\text{form}} \gtrsim 1$ .

The mean and median  $\eta$  exhibit similar behaviour, increasing with increasing  $M_{\text{vir}}$ , albeit weakly, as,

$$\langle \log_{10} \eta \rangle = 0.05 + 0.016 \log_{10} M_{12} \quad (17)$$

and

$$\text{Med } \log_{10} \eta = 0.04 + 0.019 \log_{10} M_{12}. \quad (18)$$

This means that  $\eta$  is systematically greater than unity for all  $M_{\text{vir}}$  that we consider –  $\eta \sim 1.15$  for a typical  $10^{12} h^{-1} M_{\odot}$  halo, compared to  $\eta \sim 1.25$  for a typical  $10^{15} h^{-1} M_{\odot}$  halo. The same gradual increase in  $\eta$  with decreasing  $z_{\text{form}}$  is also apparent.

As we might have anticipated from inspection of Figures 6 and 7,  $\eta'$  is systematically smaller than unity. Its variation with  $M_{\text{vir}}$  is negligible ( $\propto M_{\text{vir}}^{0.0004}$ ; a little surprising, when compared to  $\propto M_{\text{vir}}^{0.015}$  at  $z=1$ , as reported by Knebe & Power 2008) but there is a trend for the median  $\eta'$  to decrease with decreasing  $z_{\text{form}}$ . This makes sense because  $E_S$  increases with the significance of recent mergers and haloes that have had recent major mergers tend to have smaller  $z_{\text{form}}$ . This effect is also noticeable in the width of the  $\eta'$  distributions in each bin (as measured by the bars), which are larger than than the corresponding widths of the  $\eta$  distribution.

We look at this effect in more detail by plotting the distributions of  $\eta$  and  $\eta'$  shown in Figure 10. Here it is readily apparent that there is a systematic shift towards larger  $\eta$  as  $M_{\text{vir}}$  increases. Interestingly the  $\eta'$  distribution remains centred on  $\eta' \sim 0.9$ , but it spreads with increasing  $M_{\text{vir}}$ ; again, this suggests the sensitivity of  $\eta'$  to recent merging activity.

Figs. 6 to 10 demonstrate that there is a strong correlation at  $z=0$  between a halo's virial mass  $M_{\text{vir}}$ , its formation redshift  $z_{\text{form}}$  and its dynamical state, as measured by the virial ratio  $\eta$  and the centre-of-mass offset  $\Delta r$ . In contrast, the correlation with  $\eta'$  is more difficult to interpret, especially when  $\eta$  is large. In these cases, we expect significant merging activity and as we note above, the correction by the surface pressure term  $E_S$  increases the width of the original  $\eta$  distribution by a factor of  $\sim 2$ -3. It's also noteworthy that the median  $\eta'$  is systematically offset below unity. For this reason we argue that  $\eta'$  is not as useful a measure of a halo's dynamical state as  $\eta$ .

## 5 LINKING MASS ASSEMBLY AND DYNAMICAL STATE

We have established quantitative measures of a halo's mass assembly and merging history and its dynamical state in the previous two sections, and we have investigated how these relate separately to a halo's virial mass  $M_{\text{vir}}$  and its formation redshift  $z_{\text{form}}$ . In this final section we examine the relationship between a halo's mass assembly history and its dynamical state directly.

In Figures 11 and 12 we show explicitly how a halo's recent mass accretion and merging history impacts on its virial ratio. As in section 3, we quantify a halo's mass accretion history by  $(\Delta M/M)_{\tau_{\text{dyn}}}$ , the fractional increase in a halo's mass over the period  $\tau_{\text{dyn}}$  (equivalent to a redshift interval  $\Delta z \simeq 0.6$  at  $z=0$ ), and  $\alpha$ , the mean accretion rate over the period  $\tau_{\text{dyn}}$ . We use  $\delta_{\text{max}}$ , the mass ratio of the most significant merger experienced by the halo over  $\tau_{\text{dyn}}$ , to characterise a halo's recent merging history.

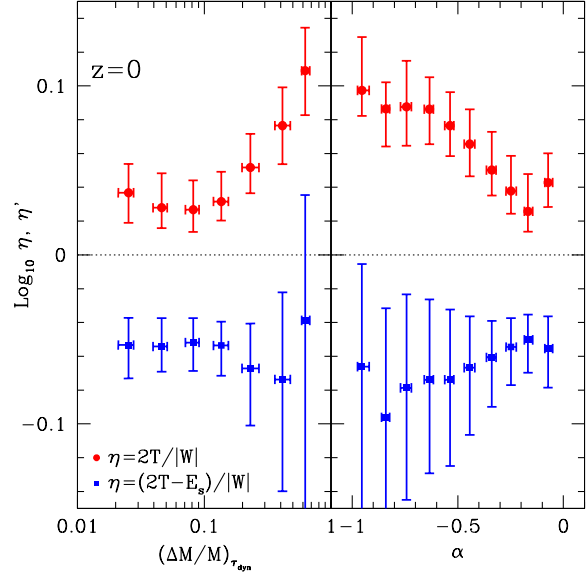


**Figure 11. Relationship between Recent Mass Accretion and the Virial Ratio.** Here we investigate how  $(\Delta M/M)_{\tau_{\text{dyn}}}$ , the fraction of mass accreted over  $\tau_{\text{dyn}}$  (left hand panel), and  $\alpha$ , the mean accretion rate over  $\tau_{\text{dyn}}$  (right hand panel), correlate with the standard ( $\eta$ , filled circles) and corrected ( $\eta'$ , filled squares) virial ratio. Data points correspond to medians and bars correspond to the upper and lower quartiles.

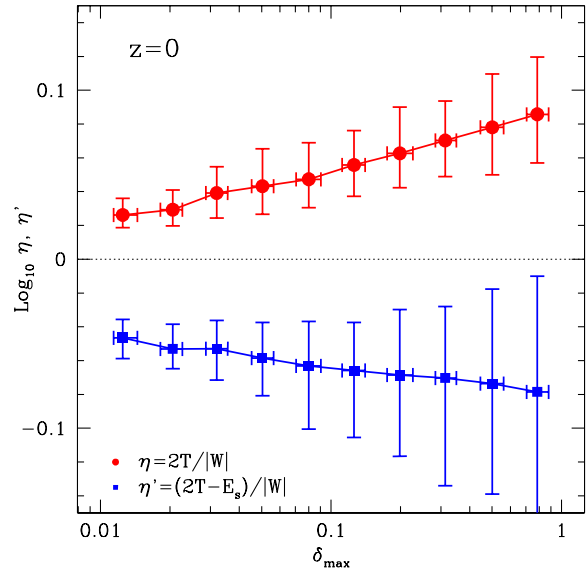


**Figure 12. Relationship between Most Significant Recent Merger and the Virial Ratio.** Here we investigate how  $\delta_{\text{max}}$ , which measures the mass ratio of the most significant recent merger since  $z=0.5$ , correlates with the standard ( $\eta$ ) and corrected ( $\eta'$ ) virial ratios respectively. Filled circles (squares) correspond to medians of  $\eta$  ( $\eta'$ ), while bars indicate the upper and lower quartiles.

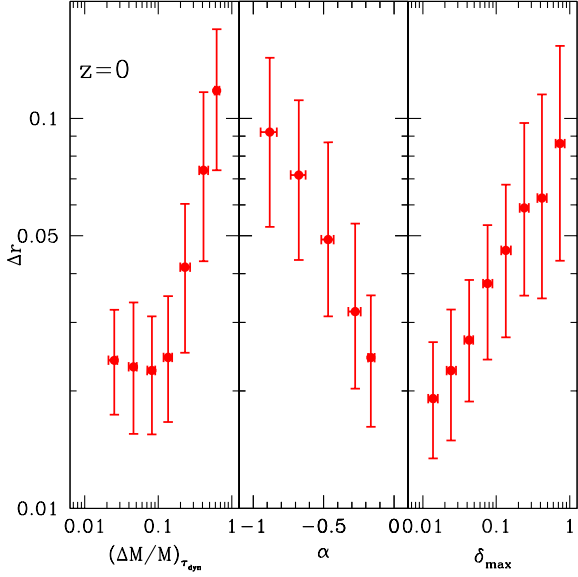


**Figure 13. Correlation between centre-of-mass offset  $\Delta r$  and Recent Merging and Accretion History.** Here we examine whether  $\Delta r$  correlates with the fraction of mass accreted over  $\tau_{\text{dyn}}$ ,  $(\Delta M/M)_{\tau_{\text{dyn}}}$ , the mean accretion rate  $\alpha$  and the most significant merger  $\delta_{\text{max}}$ . Filled circles correspond to medians in the respective bins; bars represent the upper and lower quartiles of the distribution.

We expect that the standard virial ratio  $\eta$  should increase with increasing mass accretion rate and decreasing mass ratio of most significant merger, which is in good agreement with the behaviour that we observe. In particular, the median variation of  $\eta$  with  $\alpha$  and  $\delta_{\text{max}}$  can be well approximated by  $\log_{10} \eta \simeq 0.004 - 0.126\alpha$  and  $\eta \simeq 1.2\delta_{\text{max}}^{1.1}$ ; the corresponding variation of  $\Delta r$  can be well approximated by  $0.01 - 0.1\alpha$  and  $0.1\delta_{\text{max}}^{0.3}$ .

Interestingly we note that the median corrected virial ratio  $\eta'$  declines with increasing mass accretion rate and mass ratio of most significant merger. Both correlations indicate that merger events lead to a state that is less virialised, but, as we have noted already, the inclusion of the surface pressure term over-corrects the virial ratio. We see in Figure 11 that for  $(\Delta M/M)_{\tau_{\text{dyn}}} \lesssim 0.2$ , both the median  $\eta$  and  $\eta'$  are flat;  $\eta \sim 1.05$  whereas the median  $\eta' \sim 0.85$ . Above  $(\Delta M/M)_{\tau_{\text{dyn}}} \sim 0.2$ , the median  $\eta$  increases sharply whereas it is the width of the  $\eta'$  distribution that shows the sharp increase. Comparison with Figure 12 provides further insight – the median  $\eta$  ( $\eta'$ ) shows a gradual increase (decrease) with increasing  $\delta_{\text{max}}$ , starting at  $\eta \sim 1.05$  ( $\eta' \sim 0.9$ ) for  $\delta_{\text{max}} \sim 0.02$ . For  $\delta_{\text{max}}=0.1$ ,  $\eta \sim 1.1$  ( $\eta' \sim 0.85$ ). However, whereas the width of the  $\eta$  distribution is largely insensitive to  $\delta_{\text{max}}$ , the width of the  $\eta'$  distribution increases rapidly, bearing out our observations in the previous section.

In Figure 13 we show how  $\Delta r$  varies with  $(\Delta M/M)_{\tau_{\text{dyn}}}$ ,  $\alpha$  and  $\delta_{\text{max}}$ . This reveals that  $\Delta r$  increases with increasing mass accretion rate and mass ratio of most significant recent merger, as we would expect. Although the scatter in the distribution is large, we can identify the remnants of recent major mergers ( $\delta_{\text{max}} \gtrsim 30\%$ ) as haloes with  $\Delta r \gtrsim 0.06$ . Haloes that have had relatively quiescent recent mass accretion histories ( $(\Delta M/M)_{\tau_{\text{dyn}}} \lesssim 0.1$ ,  $\delta_{\text{max}} \lesssim 10\%$ ) have  $\Delta r \lesssim 0.04$ .

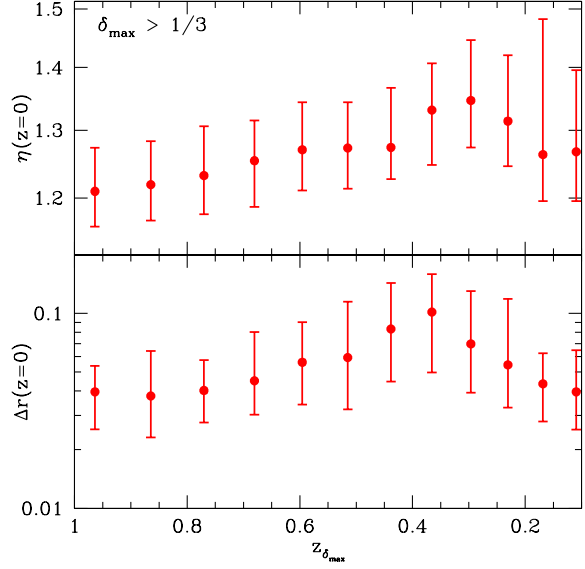


**Figure 14. Relationship between  $\eta$ ,  $\Delta r$  and  $z_{\delta_{\text{max}}}$ , the redshift of the most significant recent major merger.** We identify all haloes in our sample at  $z=0$  with  $\delta_{\text{max}} \gtrsim 1/3$  and identify the redshift  $z_{\delta_{\text{max}}}$  at which  $\delta_{\text{max}}$  occurred. Both  $\eta$  and  $\Delta r$  are evaluated at  $z=0$ . Filled circles and bars correspond to medians and upper and lower quartiles.

**Merging Timescale & Dynamical State** We conclude our analysis by investigating the timescale over which the effect of a merger can be observed in the virial ratio  $\eta$  and the centre-of-mass offset  $\Delta r$ .

In Figure 14 we investigate how a typical halo's  $\eta$  (upper panel) and  $\Delta r$  (lower panel), measured at  $z = 0$ , correlates with the redshift at which the halo suffered its most significant merger,  $z_{\delta_{\text{max}}}$ . For clarity, we focus on haloes for which  $\delta_{\text{max}} > 1/3$ , although we have verified that our results are not sensitive to the precise value of  $\delta_{\text{max}}$  that we adopt; filled circles correspond to medians and bars indicate upper and lower quartiles. The median  $\eta$  increases with decreasing  $z_{\delta_{\text{max}}}$  for  $z_{\delta_{\text{max}}} \gtrsim 1$  before peaking at  $z_{\delta_{\text{max}}} \simeq 0.3$  and declining at lower  $z_{\delta_{\text{max}}}$ . The median  $\Delta r$  shows a similar steady increase with decreasing  $z_{\delta_{\text{max}}}$  below  $z_{\delta_{\text{max}}} \sim 0.8$  although there is evidence that it peaks at  $z_{\delta_{\text{max}}} \simeq 0.4$  before declining at lower  $z_{\delta_{\text{max}}}$ . The redshift interval corresponding to  $z_{\delta_{\text{max}}} \simeq 0.3$  represents a time interval of  $\Delta t \simeq 4.3$  Gyrs or  $\sim 1.5 \tau_{\text{dyn}}$ .

This is consistent with the finding of Tormen et al. (1997), who examined the velocity dispersion  $v_{\text{rms}}$  of material within  $r_{\text{vir}}$  of simulated galaxy cluster haloes (see their Figure 5). They noted that merging leads to an increase in  $v_{\text{rms}}$  of the main (host) halo because the merging sub-halo acquires kinetic energy as it falls in the potential well of the more massive main halo. The peak in  $v_{\text{rms}}$  corresponds to the first pericentric passage of the subhalo, after which  $v_{\text{rms}}$  declines because subsequent passages are damped, and so the main halo relaxes. This will occur on a timescale of order  $\sim 1 - 2 \tau_{\text{dyn}}$ , which is consistent with the peak in  $\eta$  at  $z_{\delta_{\text{max}}} \simeq 0.3$ . We would expect to see a peak in  $\Delta r$  on roughly the merging timescale  $\tau_{\text{merge}}$ , which as we noted in § 3 is comparable to  $1 - 2 \tau_{\text{dyn}}$  (cf. Boylan-Kolchin et al. 2008).

We can take this analysis a little further by looking at the detailed evolution of  $\eta$  and  $\Delta r$  over time. In Figure 15 we plot the red-

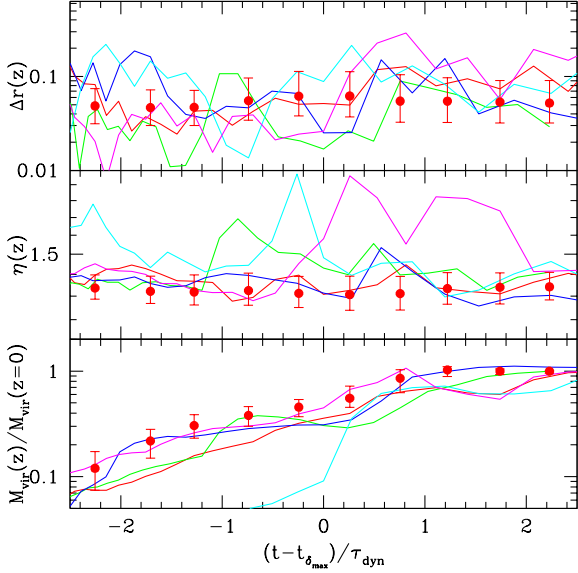


**Figure 15. Response of  $M_{\text{vir}}$ ,  $\eta$  and  $\Delta r$  to a major merger.** We include all haloes with  $\delta_{\text{max}} \gtrsim 1/3$  at  $z=0$  and plot the redshift variation of  $M_{\text{vir}}$ ,  $\eta$  and  $\Delta r$  against the time since the major merger, normalised by the dynamical time of the halo at the redshift at which the merger occurred. Filled circles and bars correspond to medians and upper and lower quartiles, while curves correspond to the histories of 5 individual haloes.

shift variation of  $M_{\text{vir}}$  (normalised to its value at  $z=0$ ; lower panel),  $\eta$  (middle panel) and  $\Delta r$  (upper panel) against the time since major merger, normalised by the dynamical time  $\tau_{\text{dyn}}$  estimated at the redshift at which the merger occurred,  $z_{\delta_{\text{max}}}$ . Medians and upper and lower quartiles are indicated by filled circles and bars. For illustrative purposes, we show also the redshift variation of  $M_{\text{vir}}$ ,  $\eta$  and  $\Delta r$  for a small subset of our halo sample (red, blue, green, cyan and magenta curves). As in Figure 14, we adopt  $\delta_{\text{max}} \gtrsim 1/3$ .

Our naive expectation is that both  $\eta$  and  $\Delta r$  should increase in response to the merger, peak after  $\Delta t \simeq \tau_{\text{dyn}}$  and then return to their pre-merger values. If this behaviour is typical, then we expect pronounced peaks in the median values of  $\eta$  and  $\Delta r$  at  $\Delta t/\tau_{\text{dyn}} \simeq 1$ . However, it is evident from Figure 15 that there is no significant difference between the median  $\eta$  and  $\Delta r$  pre- and post-major merger, and so our naive expectation is not borne out by our results.

This is not surprising if one inspects histories for  $\eta$  and  $\Delta r$  for individual haloes, in the spirit of Tormen et al. (1997);  $\eta$  and  $\Delta r$  increase following a major merger, but the behaviour is noisy (reflecting e.g. differences in orbital parameters of merging subhaloes, the redshift dependent virial radius, dependence on environment, etc...) and the timescale of the response varies from halo to halo – simply averaging or taking the median washes any signal away. Nevertheless it is worth looking at this in more detail, which we shall do in a forthcoming paper.

## 6 SUMMARY

The aim of this paper has been to quantify the impact of a dark matter halo’s mass accretion and merging history on two measures of dynamical state that are commonly used in cosmological  $N$ -body simulations, namely the virial ratio  $\eta = 2T/|W|$  (cf. Cole & Lacey 1996) and the centre-of-mass offset  $\Delta r = |\vec{r}_{\text{cen}} - \vec{r}_{\text{cm}}|/r_{\text{vir}}$  (cf.

Crone et al. 1996; Thomas et al. 1998, 2001). The virial ratio  $\eta$  derives from the virial theorem and the expectation is that  $\eta \rightarrow 1$  for dynamically equilibrated haloes. The centre-of-mass offset  $\Delta r$  can be regarded as a substructure statistic (Thomas et al. 2001) that provides a convenient measure of how strongly a halo deviates from smoothness and spherical symmetry. We expect a halo’s dynamical state and its mass assembly history to correlate closely. Understanding how is important because the degree to which a halo is dynamically equilibrated affects the reliability with which we can measure characteristic properties of its structure, such as the concentration parameter  $c_{\text{vir}}$  (e.g. Macciò et al. 2007; Neto et al. 2007; Prada et al. 2011), and kinematics, such as the spin parameter  $\lambda$  (e.g. Gardner 2001; D’Onghia & Navarro 2007; Knebe & Power 2008). For this reason, it is desirable to establish quantitatively how well they correlate and to assess how  $\eta$  and  $\Delta r$  can help us to characterise how quiescent or violent a halo’s recent mass assembly history has been.

Our key results are that  $\eta$  and  $\Delta r$  show strong positive correlations with each other (cf. Figure 7) – as  $\eta$  increases for a halo, so too does  $\Delta r$  – and that both are useful indicators of a halo’s mass recent mass accretion and merging history. For example,  $\eta$  and  $\Delta r$  correlate strongly with  $\delta_{\text{max}}$ , which measures the significance of a halo’s recent merging activity; haloes with  $\eta \lesssim 1.1$  (cf. Figure 12) and  $\Delta r \lesssim 0.04$  (cf. Figure 13) will have quiescent recent mass assembly histories – they are unlikely to have suffered mergers with mass ratios greater than 1:10 over the last few dynamical times.

In contrast, interpreting the corrected virial ratio  $\eta' = (2T - E_s)/|W|$ , where  $E_s$  is the surface pressure energy, is problematic (at least insofar as we have implemented it here, which follows the prescription of Shaw et al. 2006 and has been applied in Knebe & Power 2008 and Davis et al. 2011). In principle,  $\eta'$  should account for the approximation that is made when we define a halo to be a spherical overdensity of  $\Delta_{\text{vir}}$  times the critical density at a particular redshift. As we noted in § 2, haloes are more complex structures than this simple working definition gives them credit for, and by defining the halo’s extent by the virial radius  $r_{\text{vir}}$  the likelihood is that material that belongs to the halo will be neglected. By correcting the virial ratio  $\eta$  for what is effectively a truncation of the true halo, the corrected virial ratio  $\eta'$  takes account of the “missing” kinetic energy. However, our results imply that the correction itself (the surface pressure energy  $E_s$ ) is sensitive to a halo’s merging history, and that it increases with increasing  $\delta_{\text{max}}$  (cf. Figure 12). For this reason we would caution against the use of  $\eta'$  to identify dynamically relaxed haloes, at least in the form that is currently used.

Interestingly, we find that systems with violent recent mass assembly histories (most significant merger with a mass ratio  $\delta_{\text{max}} \gtrsim 1/3$  between  $0 \lesssim z \lesssim 1$ ) have values of  $\eta$  and  $\Delta r$  (as measured at  $z=0$ ) that peak at  $z_{\delta_{\text{max}}} \simeq 0.3 - 0.4$ , which corresponds to a timescale of  $\sim 1.5 \tau_{\text{dyn}}$  (cf. Figure 14). This is consistent with the earlier analysis of Tormen et al. (1997), who found that the velocity dispersion  $v_{\text{rms}}$  of material within the virial radius – which is linked to the virial ratio  $\eta$  – peaks on first closest approach of the merging sub-halo with the centre of the more massive host halo. This should occur on a timescale of  $\sim 1 - 2 \tau_{\text{dyn}}$ , after which  $v_{\text{rms}}$  and  $\eta$  should dampen away. Similar arguments can be made for  $\Delta r$ . We note that these arguments can be made in a statistical sense, but if we look at the merging histories of individual haloes, the behaviour of  $\eta$  and  $\Delta r$  is much more complex, and as we demonstrate a simple timescale for their response to a major merger is difficult

to define (cf. Figure 15). We shall return to this topic in future work.

What is the significance of these results? Structure formation proceeds hierarchically in the CDM model and so we expect to find correlations between virial mass  $M_{\text{vir}}$  and formation redshift  $z_{\text{form}}$  (cf. Figure 2), which in turn result in positive correlations between  $M_{\text{vir}}/z_{\text{form}}$  and  $\eta/\Delta r$ . (cf. Figures 8 and 9). This means that more massive haloes and those that formed more recently are also those that are least dynamically equilibrated, a fact that we should be mindful of when characterising the halo mass dependence of halo properties that are sensitive to dynamical state (e.g.  $c_{\text{vir}}$  and  $\lambda$ ). It's worth noting that the correlation between  $M_{\text{vir}}$  and  $\eta$  is stronger than the correlation between  $M_{\text{vir}}$  and  $\Delta r$ ; the median  $\eta$  rises sharply with  $M_{\text{vir}}$  and there is no overlap between the width of the distributions of  $\eta$  is the lowest and highest mass bins. In contrast, the median  $\Delta r$  in the highest mass bin lies in the high- $\Delta r$  tail of the lowest mass bin.

This is interesting because  $\eta$  as it is usually calculated depends on  $W$ , which is sensitive to the precise boundary of the halo. Correcting for the surface pressure term does not appear to help, as we point out – indeed, the surface pressure term itself correlates with merging activity. This points towards an ambiguity in the use of  $\eta$  – as we note, it rarely if ever satisfies  $\eta=1$ . We discuss this point in a forthcoming paper, but we note that even in ideal situations, what one computes for  $\eta$  depends on  $r_{\text{vir}}$  (cf. Cole & Lacey 1996; Łokas & Mamon 2001) – and so applying a flat cut based on a threshold in  $\eta$  alone risks omitting massive haloes that might otherwise be considered dynamically equilibrated. For this reason we advocate the use of  $\Delta r$  in cosmological  $N$ -body simulations as a more robust measure of a halo's dynamical state; its calculation is computationally inexpensive, it is well defined as a quantity to measure, and its interpretation is both clear and straightforward. We find that  $\Delta r \lesssim 0.04$ , which corresponds to a  $\delta_{\text{max}} \lesssim 0.1$ , should be sufficient to pick out the most dynamically relaxed haloes in a simulation volume at  $z=0$ .

Although our focus has been fixed firmly on haloes in cosmological simulations, we note that our results have observational implications. Whether or not an observed system – for example, a galaxy cluster – is in dynamical equilibrium will affect estimates of its dynamical mass if we assume a luminous tracer population that is in dynamical equilibrium (e.g. Piffaretti & Valdarnini 2008). Similarly, studies that seek to reconstruct a galaxy cluster's recent merging history tend to use signatures of disequilibrium (e.g. Cassano et al. 2010). The most obvious measure of disequilibrium is the centre of mass offset  $\Delta r$ , or its projected variant. Although a more careful study in which we mock observe our haloes (and a seeded galaxy population) is needed, our results suggest that  $\Delta r$  could be used to infer the redshift of the last major merger (cf. Figures 13 and Figure 9, although care must be taken as Figure 15 reveals). Observationally, this would require measurement of, for example, projected displacements between gas and dark matter from gravitational lensing and X-ray studies. We note that Poole et al. (2006) have already tested this idea using idealised hydrodynamical simulations of mergers between galaxy clusters and found that the centroid offset between X-ray and projected mass maps captures the dynamical state of galaxy clusters well, but it is interesting to extend this idea using cosmological hydrodynamical simulations of galaxy groups and clusters. This will form the basis of future work.

## ACKNOWLEDGMENTS

CP acknowledges the support of the STFC theoretical astrophysics rolling grant at the University of Leicester. AK is supported by the *Spanish Ministerio de Ciencia e Innovación* (MICINN) in Spain through the Ramon y Cajal programme as well as the grants AYA 2009-13875-C03-02, AYA2009-12792-C03-03, CSD2009-00064, and CAM S2009/ESP-1496. He further thanks the Aluminum Group for chocolates. SRK acknowledges financial support from Swinburne University of Technology's Centre for Astrophysics and Supercomputing's visitor programme. He acknowledges support by the MICINN under the Consolider-Ingenio, SyeC project CSD-2007-00050. The simulations presented in this paper were carried out on the Swinburne Supercomputer at the Centre for Astrophysics & Supercomputing, the Sanssouci cluster at the AIP and the ALICE supercomputer at the University of Leicester.

This paper has been typeset from a  $\text{\LaTeX}$  file prepared by the author.

## REFERENCES

- Bailin J., Steinmetz M., 2005, *ApJ*, 627, 647
- Bett P., Eke V., Frenk C. S., Jenkins A., Helly J., Navarro J., 2007, *MNRAS*, 376, 215
- Boylan-Kolchin M., Ma C.-P., Quataert E., 2008, *MNRAS*, 383, 93
- Boylan-Kolchin M., Springel V., White S. D. M., Jenkins A., Lemson G., 2009, *MNRAS*, 398, 1150
- Bullock J. S., Kolatt T. S., Sigad Y., Somerville R. S., Kravtsov A. V., Klypin A. A., Primack J. R., Dekel A., 2001, *MNRAS*, 321, 559
- Cassano R., Ettori S., Giacintucci S., Brunetti G., Markevitch M., Venturi T., Gitti M., 2010, *ApJ*, 721, L82
- Chandrasekhar S., 1961, *Hydrodynamic and hydromagnetic stability*. International Series of Monographs on Physics, Oxford: Clarendon, 1961
- Cole S., Lacey C., 1996, *MNRAS*, 281, 716
- Crone M. M., Evrard A. E., Richstone D. O., 1996, *ApJ*, 467, 489
- Davis A. J., D'Aloisio A., Natarajan P., 2011, *MNRAS*, pp 950–
- Diemand J., Kuhlen M., Madau P., 2007, *ApJ*, 667, 859
- Diemand J., Kuhlen M., Madau P., Zemp M., Moore B., Potter D., Stadel J., 2008, *Nature*, 454, 735
- Diemand J., Moore B., 2009, *Arxiv e-prints* (arXiv:0906.4340)
- D'Onghia E., Navarro J. F., 2007, *MNRAS*, 380, L58
- Eke V. R., Cole S., Frenk C. S., Patrick Henry J., 1998, *MNRAS*, 298, 1145
- Fakhouri O., Ma C.-P., 2008, *MNRAS*, 386, 577
- Fakhouri O., Ma C., 2010, *MNRAS*, 401, 2245
- Fakhouri O., Ma C.-P., Boylan-Kolchin M., 2010, *MNRAS*, 406, 2267
- Gao L., Navarro J. F., Cole S., Frenk C., White S. D. M., Springel V., Jenkins A., Neto A. F., 2008, *MNRAS*, 387, 536
- Gao L., Frenk C. S., Boylan-Kolchin M., Jenkins A., Springel V., White S. D. M., 2011, *MNRAS*, 410, 2309
- Gardner J. P., 2001, *ApJ*, 557, 616
- Gill S. P. D., Knebe A., Gibson B. K., 2004, *MNRAS*, 351, 399
- Hetznecker H., Burkert A., 2006, *MNRAS*, 370, 1905

- Kendall M., Gibbons J. D., 1990, *Rank Correlation Methods*, 5 edn. A Charles Griffin Title
- Knebe A., Power C., 2008, *ApJ*, 678, 621
- Knollmann S. R., Knebe A., 2009, *ApJS*, 182, 608
- Lacey C., Cole S., 1993, *MNRAS*, 262, 627
- Li Y., Mo H. J., Gao L., 2008, *MNRAS*, 389, 1419
- Lokas E. L., Mamon G. A., 2001, *MNRAS*, 321, 155
- Macciò A. V., Dutton A. A., van den Bosch F. C., Moore B., Potter D., Stadel J., 2007, *MNRAS*, 378, 55
- Mandelbaum R., Seljak U., Hirata C. M., 2008, *Journal of Cosmology and Astroparticle Physics*, 8, 6
- Maulbetsch C., Avila-Reese V., Colín P., Gottlöber S., Khalatyan A., Steinmetz M., 2007, *ApJ*, 654, 53
- McBride J., Fakhouri O., Ma C.-P., 2009, *MNRAS*, 398, 1858
- Navarro J. F., Frenk C. S., White S. D. M., 1997, *ApJ*, 490, 493
- Navarro J. F., Ludlow A., Springel V., Wang J., Vogelsberger M., White S. D. M., Jenkins A., Frenk C. S., Helmi A., 2010, *MNRAS*, 402, 21
- Neto A. F., Gao L., Bett P., Cole S., Navarro J. F., Frenk C. S., White S. D. M., Springel V., Jenkins A., 2007, *MNRAS*, pp 922–+
- Piffaretti R., Valdarnini R., 2008, *A&A*, 491, 71
- Poole G. B., Fardal M. A., Babul A., McCarthy I. G., Quinn T., Wadsley J., 2006, *MNRAS*, 373, 881
- Power C., Navarro J. F., Jenkins A., Frenk C. S., White S. D. M., Springel V., Stadel J., Quinn T., 2003, *MNRAS*, 338, 14
- Prada F., Klypin A. A., Cuesta A. J., Betancort-Rijo J. E., Primack J., 2011, *ArXiv e-prints*
- Romano-Díaz E., Hoffman Y., Heller C., Faltenbacher A., Jones D., Shlosman I., 2007, *ApJ*, 657, 56
- Seljak U., Zaldarriaga M., 1996, *ApJ*, 469, 437
- Shaw L. D., Weller J., Ostriker J. P., Bode P., 2006, *ApJ*, 646, 815
- Springel V., 2005, *MNRAS*, 364, 1105
- Springel V., White S. D. M., Jenkins A., Frenk C. S., Yoshida N., Gao L., Navarro J., Thacker R., Croton D., Helly J., Peacock J. A., Cole S., Thomas P., Couchman H., Evrard A., Colberg J., Pearce F., 2005, *Nature*, 435, 629
- Springel V., Frenk C. S., White S. D. M., 2006, *Nature*, 440, 1137
- Springel V., Wang J., Vogelsberger M., Ludlow A., Jenkins A., Helmi A., Navarro J. F., Frenk C. S., White S. D. M., 2008, *MNRAS*, 391, 1685
- Stadel J., Potter D., Moore B., Diemand J., Madau P., Zemp M., Kuhlen M., Quilis V., 2009, *MNRAS*, 398, L21
- Thomas P. A., Colberg J. M., Couchman H. M. P., Efstathiou G. P., Frenk C. S., Jenkins A. R., Nelson A. H., Hutchings R. M., Peacock J. A., Pearce F. R., White S. D. M., 1998, *MNRAS*, 296, 1061
- Thomas P. A., Muanwong O., Pearce F. R., Couchman H. M. P., Edge A. C., Jenkins A., Onuora L., 2001, *MNRAS*, 324, 450
- Tormen G., Bouchet F. R., White S. D. M., 1997, *MNRAS*, 286, 865
- van den Bosch F. C., 2002, *MNRAS*, 331, 98
- Wechsler R. H., Bullock J. S., Primack J. R., Kravtsov A. V., Dekel A., 2002, *ApJ*, 568, 52
- White S. D. M., Rees M. J., 1978, *MNRAS*, 183, 341
- White S. D. M., Frenk C. S., 1991, *ApJ*, 379, 52
- White S. D. M., 1996, in Schaeffer R., Silk J., Spiro M., Zinn-Justin J., eds, *Cosmology and Large Scale Structure Formation and Evolution of Galaxies*. pp 349–+